ChemComm

CrossMark
← click for updates

Preparation and applications of novel composites composed of metal–organic frameworks and two-dimensional materials

Shaozhou Li,[a] Kai Yang,[b] Chaoliang Tan,[c] Xiao Huang,*[b] Wei Huang[b] and Hua Zhang*[c]

Metal–organic frameworks (MOFs), an emerging type of porous crystalline materials, have received increasing attention in recent years due to their compositional, structural and chemical versatility. More-over, great progress has been made in the fundamental study and technological development of two-dimensional (2D) materials, such as graphene and metal dichalcogenide nanosheets, which exhibit a number of unique and attractive properties for wide applications. Recently, the smart integration of the aforementioned two types of functional materials, *i.e.* MOFs and 2D materials, has led to improved performance in molecular absorption, separation and storage, and shown promise in selective catalysis and biosensing. This feature article aims at providing a brief introduction to the composites composed of MOFs and 2D materials, focusing mainly on their preparation methods and applications. Finally, technical challenges and future opportunities in this field will also be discussed.

[a] Key Laboratory for Organic Electronics and Information Displays & Institute of Advanced Materials, Jiangsu National Synergistic Innovation Center for Advanced Materials (SICAM), Nanjing University of Posts & Telecommunications, 9 Wenyuan Road, Nanjing 210023, China
[b] Key Laboratory of Flexible Electronics (KLOFE) & Institute of Advanced Materials (IAM), Jiangsu National Synergistic Innovation Center for Advanced Materials (SICAM), Nanjing Tech University (Nanjing Tech), 30 South Puzhu Road, Nanjing 211816, P. R. China. E-mail: iamxhuang@njtech.edu.cn
[c] Center for Programmable Materials, School of Materials Science and Engineering, Nanyang Technological University, 50 Nanyang Avenue, Singapore 639798, Singapore. E-mail: HZhang@ntu.edu.sg

1. Introduction

Metal–organic frameworks (MOFs) are a class of porous crystal-line materials formed by coordinating organic bridging ligands with metal ions or clusters.[1] Compared with other macromolecular materials, MOFs possess permanent porosity with tunable pore size and rich surface chemistry.[2,3] Importantly, given the wide choice of metal ions and ligands, MOFs can be rationally designed and synthesized with a broad range of structural,

Shaozhou Li

Shaozhou Li received his Bachelor Degree from the Huazhong University of Science & Technology in 2003, Master Degree from the National University of Singapore in 2004 and completed his PhD at the Nanyang Technological University in 2011. He is now a professor in the School of Materials Science & Engineering at the Nanjing University of Posts & Telecommunications. His research interests include the synthesis and application of hybrid materials based on nanostructures and metal–organic framework materials.

Xiao Huang

Xiao Huang received her Bachelor Degree from the School of Materials Science and Engineering of Nanyang Technological University in Singapore in 2006 and completed her PhD under the supervision of Professor Hua Zhang and Professor Freddy Boey in 2011. After that, she worked as a postdoctoral fellow in Professor Hua Zhang's group. She is now a professor at the Institute of Advanced Materials of Nanjing Tech University in China. Her research interest includes the synthesis and applications of two-dimensional nanomaterial-based hybrid structures.

electrical, optical, magnetic and catalytic properties.[4–8] These attractive features make MOFs promising candidates not only in the conventional areas of gas storage,[9] molecular separation[10] and catalysis,[11] but also in other fields such as bio/chemical sensing,[8,12] light emission and biomedicine.[13,14] Moreover, the application of MOFs has also been further broadened by incorporating them with other functional species to form MOF-based composites.[15–19]

Two-dimensional (2D) materials, constructed from one or a few layers of atoms, have attracted significant attention over the past decade.[20–22] Since the exfoliation of graphene and the demonstration of its outstanding electrical properties by Geim *et al.* in 2004,[23] graphene and graphene-like 2D materials as well as their applications in electronics, optoelectronics, thermoelectrics, and catalysis have been investigated.[24–30] More recently, 2D organic or metal–organic materials, such as MOF and COF nanosheets, have also attracted considerable attention.[31] Considering the unique physical and chemical properties of MOFs and 2D materials, their hybridization is anticipated to impart unique properties for various applications. For example, the integration of 2D materials, such as graphene or metal sulphide nanosheets, with MOFs can improve the electrical conductivity of the non-conductive MOF matrix.[32] Moreover, embedding 2D materials in MOF matrices can prevent the aggregation of 2D materials and retain their large surface area, which is essential for many electrical and electrochemical applications.[33,34]

The research related to MOFs or 2D materials has increased dramatically over the past two decades, and many review articles have been published that focus on the synthesis, chemical modification and applications of MOFs or 2D materials.[21,35–42]

Hua Zhang obtained his BSc and MSc degrees at Nanjing University in 1992 and 1995, respectively, and completed his PhD supervised by Professor Zhongfan Liu at the Peking University in 1998. As a Postdoctoral Fellow, he joined Prof. Frans C. De Schryver's group at Katholieke Universiteit Leuven (Belgium) in 1999, and then moved to Prof. Chad A. Mirkin's group at Northwestern University in 2001. After he worked at NanoInk Inc. (USA) and Institute of Bioengineering and Nanotechnology (Singapore), he joined Nanyang Technological University in July 2006. His current research interests focus on synthesis of ultrathin two-dimensional nanomaterials (e.g. metal nanosheets, graphene, metal dichalcogenides, metal–organic frameworks, and black phosphorus) and their hybrid composites for various applications in nano- and biosensors, clean energy, (opto-)-electronic devices, catalysis, and water remediation; controlled synthesis, characterization and application of novel metallic and semiconducting nanomaterials, and complex heterostructures.

Hua Zhang

Currently, there is increasing research interest in the synthesis and applications of 2D material/MOF composites, which has not been reviewed yet. Therefore, this review will aim to fill this gap and discuss the preparation, properties and applications of 2D material/MOF composites. First, strategies employed to prepare 2D material/MOF composites are introduced. Then, their potential applications are discussed. Finally, the current challenges and future opportunities for 2D material/MOF composites and prospects for their applications are presented.

2. Preparation of 2D material/MOF composites

Over the past couple of years, different methods have been developed for the preparation of 2D material/MOF hybrid structures. Most of these methods are solution-based using dispersions of 2D materials as starting materials, which are prepared by exfoliation of their bulk layered crystals. Subsequently, MOF materials can be hybridized with 2D materials by either the *in situ* crystallization or physical mixing method. In the following content, these methods will be discussed in detail.

2.1 *In situ* growth of MOFs on 2D materials

2D materials have been proven effective templates to assist the *in situ* growth of various inorganic nanocrystals, including metals, metal oxides, and metal sulfides.[37] Similarly, the *in situ* growth method has also been widely applied to prepare 2D material/MOF composites. In a typical process, 2D materials with surface charges or functional groups were dispersed in a solution containing metal ions and ligands to initiate the crystallization of MOFs either at room temperature or at elevated temperature.

Among various 2D materials, graphene oxide (GO) has abundant oxygen-containing groups, such as hydroxyl and carboxylic groups, on its surface, which are favourable for promoting the heterogeneous nucleation of MOF crystals on 2D nanosheets. For example, GO/MOF-5 composite was prepared by dispersing GO sheets into the growth solution of MOF-5, followed by a solvothermal treatment.[43] The resultant GO/MOF-5 composite showed a thin platelet morphology similar to that of the pure MOF-5 crystal. Other GO/MOF composites, such as GO/Cu-MOF, GO/rare-earth MOF (*e.g.* La-MOF), GO/ZIF-8, GO/MOF-253 and GO/MIL-101, have also been synthesized *via* a similar procedure.[44–48]

Owing to the rich carbon-based chemistry, chemically derived graphene, *i.e.* GO or reduced GO (rGO), can be further modified with desired functional groups *via* diversified methods.[49,50] As a result, various ligands can be linked to graphene basal surfaces, which in turn react with metal ions or connect to other ligands. In this way, hybrid MOF structures can be obtained with periodically intercalated graphene sheets. As a typical example, Loh and coworkers reported the growth of MOF-5 on benzoic acid functionalized graphene (BFG), which acted as a structure-directing agent to effect the crystal growth of MOF-5 (Fig. 1a).[51] Interestingly, it was found that the morphology
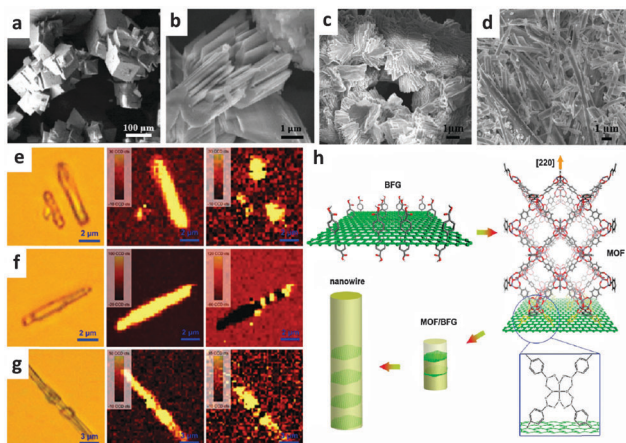
Fig. 1 (a–d) SEM images for (a) MOF-5, (b) MOF/BFG (1 wt%), (c) MOF/BFG (4 wt%) and (d) MOF/BFG (5 wt%). (e–g) Raman mapping of MOF/BFG nanowires. Left: Optical image; middle: Raman maps integrated by Raman band at 1609 cm^{-1}; right: Raman maps integrated by D band of graphene. (h) Schematic of proposed bonding between the functionalized graphene and MOFs *via* COOH groups along the [220] direction, and their assembly into nanowire structure. Reprinted with permission from ref. 51. Copyright 2010 American Chemical Society.
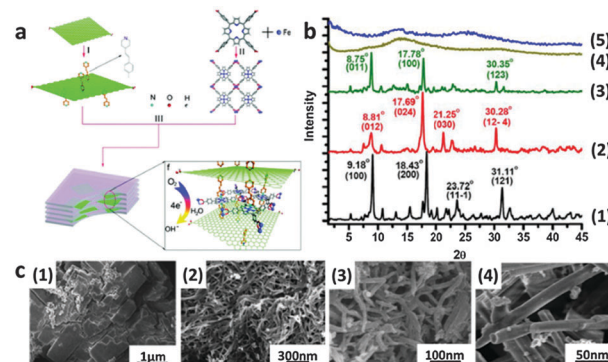

Fig. 2 (a) Schematic of the formation of hybrid MOF-2D material structures. (b) XRD patterns of $(Fe–P)_n$ MOF (1), (G-dye 5 wt%–FeP)$_n$ MOF (2), (G-dye 10 wt%–FeP)$_n$ MOF (3), (G-dye 25 wt%–FeP)$_n$ MOF (4) and G dye (5). (c) SEM images for $(Fe–P)_n$ MOF (1), (G-dye 5 wt%–FeP)$_n$ MOF (2), (G-dye 10 wt%–FeP)$_n$ MOF (3 and 4), (G-dye 25 wt%–FeP)$_n$ MOF (5), and G-dye (6). Reprinted with permission from ref. 55. Copyright 2012 American Chemical Society.

of the composite changed with the weight ratio of BFG. At low concentration of BFG (*e.g.* 1 wt%), the BFG layers were inserted in the cubic crystal of MOF/BFG (Fig. 1b), while as the BFG content increased to 5 wt%, the MOF/BFG composite underwent a dramatic morphology transformation from cubes to nanowires (Fig. 1a–d). The nanowires were further investigated by micro-Raman spectroscopy (Fig. 1e–g), which showed that the majority of the BFG flakes in MOF/BFG nanowires were distributed at the nanowire tips, periodically distributed along the nanowires, or along the entire nanowires. On the basis of the structural analysis combined with the fact that the main functional groups on the basal planes of BFG are phenyl carboxylic groups, Loh and coworkers proposed that the nucleation of MOF-5 began with the anchoring of zinc oxide clusters on BFG *via* metal–carboxylate bonding (Fig. 1h). This is similar to the previously reported oriented growth of MOF crystals on self-assembled monolayers (SAMs) covered substrates.[52,53] Furthermore, the 2D pillared bi-layer MOF (Cd-PBM) {[Cd$_4$(azpy)$_2$(pyrdc)$_4$(H$_2$O)$_2$]·9H$_2$O$_n$ (azpy = 4,4′-azopyridine, pyrdc = pyridine-2,3-dicarboxylate)} was also prepared on BFG sheets by a similar process.[54] Compared to the pristine Cd-PBM MOF, which displays a faceted particulate morphology, the BFG–Cd-PBM hybrid exhibits a plate-like morphology with large lateral dimensions.[54]

In addition to the aforementioned morphology change of MOF crystals induced by graphene, it was also observed by Loh's group that the structural property of MOF crystals can also be altered on functionalized graphene sheets.[55] In particular, as shown in Fig. 2a, the (G-dye–FeP)$_n$ MOF composite was synthesized by integration of pyridinium moieties-functionalized rGO sheets (denoted as G-dye) with $(Fe–P)_n$, a MOF created by linking 5,10,15,20-tetrakis(4-carboxyl)-21H,23H-porphyrin (TCPP) and FeCl$_3$. The intercalation of G-dye in the composite resulted in lattice distortion of the $(Fe–P)_n$ MOF segments, leading to the

gradual transformation of crystalline MOF into an amorphous solid, as indicated by systematic X-ray diffraction (XRD) analysis (Fig. 2b). Accompanying the change in crystal structure, the morphology of $(Fe–P)_n$ MOF crystals also transformed from plates to rods as the G-dye content increased (Fig. 2c). Following this work, the same group synthesized a GO-intercalated copper-centered MOF composite.[56] Again, with increasing GO content, the original Cu-MOF with a tetragonal crystal structure (space group: P4/ncc) gradually transformed to the tetragonal structure (space group: P4/mbm). A marked change in the morphology of (GO x wt%) Cu-MOF crystal from faceted to layered structures also occurred when the concentration of GO incorporated in the MOF structure gradually increased to 8 wt%. It was suggested that the twisting of ligand, *i.e.* 1,4-benzenedicarboxylic acid (bdc), which was covalently bound to the hydroxyl or epoxy groups on GO, was likely the cause of the observed morphological and structural change in the Cu-MOF crystal.

Not only graphene and its derivatives have been hybridized with MOFs, other inorganic 2D materials, such as MoS$_2$ and boron nitride (BN), have also been applied as flexible templates to support the growth of MOFs. However, it should be noted that unlike graphene derivatives, there are no functional groups on the surfaces of pristine MoS$_2$ and BN, resulting in difficulty of growth of MOF crystals on them.[57,58] Fortunately, the MoS$_2$ nanosheets prepared by a chemical or electrochemical Li-intercalation method are negatively charged, making them easy to absorb metal ions *via* electrostatic interaction.[59] By using such negatively charged nanosheets as a template, our group demonstrated the continuous coating of a thin layer of ZIF-8 MOF on MoS$_2$ or Pt NP-coated MoS$_2$, denoted as MoS$_2$@ZIF-8 or Pt-MoS$_2$@ZIF-8, respectively.[60] These core–shell structures were confirmed by transmission electron microscopy (TEM) and energy dispersive spectroscopy (EDS). For example, for the ternary hybrid Pt-MoS$_2$@ZIF-8, it was clearly observed from the TEM image that Pt NPs, which were coated on MoS$_2$ nanosheets, were well-embedded in the MOF shell (Fig. 3a–d).
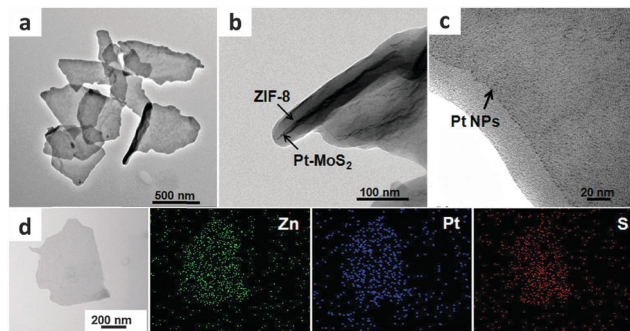
Fig. 3 (a–c) TEM images of (a) Pt-MoS$_2$@ZIF-8 hybrid structures, (b) a curled Pt-MoS$_2$@ZIF-8 structure, showing the embedded Pt-MoS$_2$ core and ZIF-8 shell, (c) the edge area of a Pt-MoS$_2$@ZIF-8 structure, revealing the embedded Pt NPs, and (d) STEM image and the corresponding EDS mapping of a typical Pt-MoS$_2$@ZIF-8 hybrid structure. Reprinted with permission from ref. 60. Copyright 2014 American Chemical Society.

As demonstrated by Coleman *et al.* in 2011, by using a suitable polar solvent, numerous 2D nanosheets can be obtained by the ultrasonication-assisted liquid exfoliation method.[26] For example, BN nanosheets can be ultrasonically exfoliated from its bulk crystal in dimethylformamide (DMF). However, it was found by Zhao and coworkers that when BN nanosheets in DMF were directly mixed with the precursors for growth of MIL-53(Al), the precursors interacted more strongly with DMF molecules rather than with BN, resulting in the preferred nucleation of MIL-53 in the solution instead of on the BN surface. To solve this problem, they used a so-called "double-solvent replacement method", in which water was used to replace DMF, to grow MIL-53(Al). Surprisingly, in the aqueous solution, the Al^{3+} ions bound strongly on the BN nanosheets, which enabled BN as a structure-directing template to guide the growth of MIL-53(Al), and the obtained composite showed a hierarchically layered structure containing both BN nanosheets and MOF crystals.[61]

2.2 Physical mixing of MOFs and 2D materials

Physically mixing the pre-synthesized MOF crystals and 2D nanosheets is another commonly used method to prepare 2D material/MOF composites. Compared to the aforementioned *in situ* growth methods,[51,59] the physical mixing method is simple and more predictable and controllable on MOF structures. For example, the GO/copper terephthalate (Cu(TPA)) MOF composite was prepared by simply stirring and ultrasonicating a solution containing GO sheets and Cu(TPA) MOF crystals.[62] Due to the coupling of π electrons between the terephthalate linkers in Cu(TPA) MOFs and unoxidized aromatic rings in GO sheets, the Cu(TPA) and GO strongly bonded together and the resultant composite showed excellent chemical stability in water. In another report, *via* the simple electrostatic interaction, Zhao *et al.* prepared a graphene-wrapped MIL-101 composite, which was then used as a cathode for a Li–S battery through directly mixing the sulfur infiltrated MIL-101(Cr) and graphene. In this hybrid composite, the large surface area and pore volume of MIL-101(Cr) ensured a high dispersion of sulfur, and the graphene-wrapped MIL-101(Cr) layers minimized the loss of

polysulfides into the electrolyte during the charging process in the battery.[63]

3. Applications of 2D material/MOF composites

3.1 Absorption, storage and separation of molecules

Like many conventional porous solids, such as silica and zeolite, MOFs are excellent candidates for absorption, storage and separation of molecules, owing to their high surface area, controllable porosity and size/shape-tunable cavity. For example, several studies have demonstrated applications of MOFs and their composites in the storage and separation of methane or H$_2$ for fuel cells.[64,65] In addition, MOFs are also attractive materials for absorption and removal of gases such as CO$_2$, NH$_3$, H$_2$S and NO$_2$ for environmental remediation.[66,67]

Moreover, 2D materials, especially graphene-based materials, can be fabricated into hierarchically porous structures with high surface area and tunable surface properties *via* doping or chemical functionalization, which are then used for gas absorption and storage.[68,69] It is demonstrated that the combination of MOFs and 2D materials has led to further enhanced performance in molecule absorption and storage.[70–78]

Driven by the increasing level of atmospheric CO$_2$, the capture and storage of CO$_2$ have become a very important application for porous solid materials. It has been observed that in several GO/MOF hybrid systems, after the incorporation of GO nanosheets with MOFs, their capability in CO$_2$ capture was greatly improved. For example, Rao and coworkers reported that the CO$_2$ uptake at 195 K dramatically increased from 27.2 wt% in pure ZIF-8 and 33 wt% in pure GO to 72 wt% in ZIF-8 hybridized with 20 wt% GO.[70] A similar phenomenon has also been observed in GO/Cu-MOF[71] and GO/MIL-101(Cr)[72] composites. One possible explanation for the improved CO$_2$ uptake is attributed to the synergistic effect arising from the formation of abundant active sites at the MOF/GO interface for the reactive adsorption of CO$_2$.

The improved gas adsorption capacity is realized not only for CO$_2$ uptake, but also for the adsorption of other gases such as H$_2$, which is currently one of the most important green energy sources. For example, at 77 K and 42 atm, the GO/Cu-MOF composite possesses a H$_2$ storage capacity of 3.58 wt%, which is higher than that of pure Cu-MOF, with its storage capacity of 2.81 wt%.[71] H$_2$ uptake capacity can be further improved by deposition of Pt NPs on the surface of the MOF/GO composite through the "spillover" effect.[73] Based on this effect, the hydrogen molecules on the Pt NP surface can be split *via* dissociative chemisorption to obtain hydrogen atoms.[74] Because hydrogen atoms are more easily absorbed compared to hydrogen molecules, the hydrogen uptake on Pt NP/MOF/GO can be improved significantly. Indeed, in a series of works conducted by Zhou *et al.*,[75–77] several types of Pt-doped MOF/GO hybrids, such as Pt/GO/Cu-MOF, Pt/GO/ZIF-8 and Pt/GO/MIL-101, used for H$_2$ storage showed up to 3 times
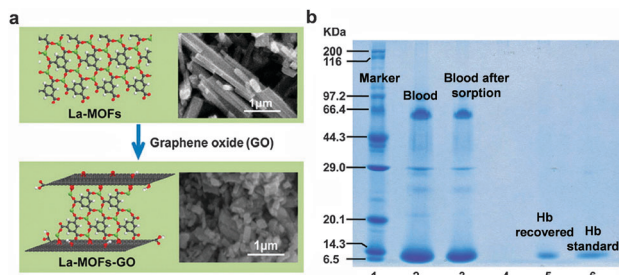
Fig. 4 (a) Schemes and SEM images of formation of La-MOF–GO composites. The rectangular rod-shaped La-MOFs (upper SEM image) became short and block-like (bottom SEM image) in the presence of GO sheets. (b) SDS-PAGE assay results. Lane 1: molecular weight standards (markers in kDa); lane 2: 100-fold diluted human whole blood without pretreatment; lane 3: 100-fold diluted human whole blood after adsorption by La-MOF–GO composite; lane 4: washing solution by deionized water; lane 5: Hb recovered from the La-MOF–GO composite; lane 6: Hb standard solution of 150 mg L^{-1}. Reprinted with permission from ref. 47. Copyright 2014 American Chemical Society.

increased storage capacity compared to the MOF/GO composite without Pt loading.

In addition to the absorption of small gas molecules, MOF-based composites have also been used as the absorbents for larger molecules such as dye molecules[78] and proteins.[47] For example, Liu *et al.* reported the use of the GO/La-MOF (La(BTC)(H$_2$O)$_6$) composite (Fig. 4a) for adsorption of proteins, *e.g.* hemoglobin (Hb). The phenyl-rich ligands in the La-MOF enabled strong π–π interaction between the amino acid residues in proteins and the surface of MOFs. In addition, the conjugate π-electron moieties in GO also contribute to the protein adsorption. More importantly, the selective absorption of Hb is realized against other proteins such as bovine serum albumin (BSA) because of the strong face-to-face π–π interaction between the heme moieties in Hb and the GO/La-MOF composite.[47] Fig. 4b shows the selective absorption of Hb from a whole blood sample, indicating that the GO/MOF hybrid might be a promising absorbent for selective extraction of proteins from biological samples of complex matrixes.

Moreover, 2D material/MOF composites can also be fabricated into membranes for molecule separation. Owning to the well-defined pore size in MOF crystals, these hybrid membranes can realize size-selective molecular separation, meaning that small molecules can pass through the pores/cavities, while big ones are blocked outside the pores. For example, Huang *et al.* reported that the GO/ZIF-8 membrane showed high hydrogen selectivity against the relatively larger gas molecules such as CO$_2$, N$_2$ and CH$_4$.[48] At 250 °C and 1 bar, the separation factors for gas mixtures H$_2$/CO$_2$, H$_2$/N$_2$, H$_2$/CH$_4$, and H$_2$/C$_3$H$_8$ are 14.9, 90.5, 139.1, and 3816.6, respectively, along with the high H$_2$ permeances of up to 1.3×10^{-7} mol m^{-2} s^{-1} Pa^{-1}. Importantly, even in the presence of steam, the GO/ZIF-8 membrane consistently displayed high stability with unchanged H$_2$ permeance and H$_2$/CH$_4$ selectivity for at least 72 h.

In addition to the size selective effect, another important factor that controls the selectivity of a membrane is its surface affinity for target molecules. For instance, CO$_2$ shows stronger

binding ability on GO surface compared to CH$_4$ due to its relatively high quadrupole moment. As a result, the GO/MIL-101(Cr) composite reported by Zhou *et al.* exhibited a much enhanced adsorption selectivity for CO$_2$/CH$_4$ of up to 32 at room temperature.[72]

3.2 Catalysis

Perhaps one of the most detrimental problems that restrict the wide application of nanostructured catalysts is the reduced surface area caused by aggregation/re-stacking during the catalytic process. Incorporation of catalysts in a porous matrix, such as MOF, is expected to counter this problem by effectively keeping the nanomaterials well separated from each other.[80] Moreover, the porous channels of MOF crystals also ensure the accessibility of active surfaces of the embedded catalysts to ions/gases. Moreover, the MOF matrix with its uniform pore/channel size enables size-selective catalytic reactions by selectively permeating target ions/gases to reach the catalyst surface. For example, Zhang's group demonstrated that the ZIF-8 coated Pt nanoparticle–rGO composite can be used to selectively catalyze the liquid-phase hydrogenation of *n*-hexene *versus cis*-cyclooctene, which showed selective conversion efficiencies of 21% and 4.8% for *n*-hexene and *cis*-cyclooctene, respectively.[60]

In fact, many MOFs are natural catalysts with active metal centers. However, some of them crystallize preferentially into large crystals with sizes of up to a few micrometers. The inner surface of the crystals cannot be easily accessed by ions/gases during the catalytic process, which greatly reduces the catalyst efficiency. As mentioned in the previous section, Wang *et al.* used the BN nanosheet as a template to direct the *in situ* growth of MIL-53 to form the plate-like structure with a thickness of less than 100 nm.[61] The reduced dimension enabled more catalytic centers in MIL-53 accessible to ions/gases. As a proof-of-concept demonstration, they used this hybrid material to catalyze the acetalization of benzaldehyde at room temperature[61] and found that BN/MIL-53 showed 70.4% conversion of benzaldehyde, while pure MIL-53 showed less than 50% conversion under the same experimental conditions.

In addition to organic catalysis, MOF composites have also been used for electrocatalysis. Although many MOF materials are electrochemically active, most of them are poor conductors,[79] as the metal nodes are not in a redox-active form and most organic ligands used for constructing MOFs do not facilitate electron transfer. Hence, strategies have been developed to synthesize conductive MOFs using redox-active metal centers or/and organic linkers,[81] or electron donor/acceptor building blocks.[82] Alternatively, it would be much easier to directly hybridize MOFs with conductive materials such as rGO.[83] By using the chemically modified GO as the intercalating backbone layer of MOF, Loh *et al.* reported that the graphene–porphyrin MOF composite exhibited good electrocatalytic activity towards the oxygen reduction reaction (ORR) in an alkaline medium with an onset potential of *ca.* 0.93 V *vs.* RHE.[55] Compared to the commercial Pt catalyst, this porphyrin–MOF composite possesses much higher selectivity for ORR and significantly
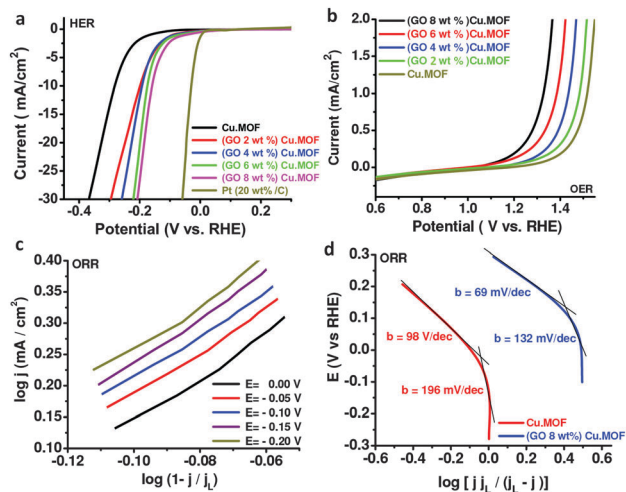
Fig. 5 (a) Performance of hydrogen evolution reaction with various catalysts. LSV polarisation curves of Pt/C, (GO 2, 4, 6, and 8 wt%) Cu-MOF, and Cu-MOF in 0.5 M H$_2$SO$_4$, N$_2$-saturated; scan rate: 2 mV s^{-1} at 25 °C. (b) Performance of oxygen evolution reaction with various catalysts. LSV polarisation curves for Cu-MOF, (GO 2, 4, 6, and 8 wt%) in N$_2$-saturated 0.5 M H$_2$SO$_4$; scan rate: 2 mV s^{-1} at 25 °C. (c) Plots for the determination of the reaction order with respect to O$_2$ for ORR on (GO 8 wt%) Cu-MOF electrode. (d) Mass transfer-corrected Tafel plots for ORR on (GO 8 wt%) Cu-MOF and Cu-MOF electrodes. Reprinted with permission from ref. 56. Copyright 2013 John Wiley & Sons, Inc.

reduced methanol crossover effect. Following this work, they also found that the GO-copper centered MOF composite exhibited smaller overpotential and higher current for all three electrocatalytic reactions, e.g., hydrogen evolution reaction (HER) (Fig. 5a), oxygen evolution reaction (OER) (Fig. 5b) and ORR (Fig. 5c and d), compared to the intrinsic Cu-MOF.[53] Importantly, the GO-incorporated Cu-MOF composite can deliver power density that is 76% of that of a commercial Pt catalyst tested in a polymer electrolyte membrane fuel cell, making it an ideal low-cost substitute to noble metal catalysts. In another example, Xu et al. used the graphene/Prussian blue (PB) composite as the catalyst for four-electron oxygen reduction in an acidic medium.[84] Rotation disk electrode (RDE) voltammetric measurements implied that both PB and graphene are important in the ORR; that is, at $E > -0.5$ V, ORR occurs mainly inside the PB lattice through the 4-electron reduction pathway, and at $E < -0.5$ V, ORR takes place on graphene sheets with H$_2$O$_2$ as the intermediate product.

The versatility of MOFs lies not only in their structural and chemical properties, but also in their electrical properties. Especially, many MOFs are semiconducting materials with suitable bandgaps for solar energy conversion. However, the single-component photocatalyst usually suffers from the fast recombination of charge carriers, resulting in reduced energy harvesting efficiency. To overcome this, graphene or chemically modified graphene nanosheets can be used to improve charge carrier transport.[85] For example, when MIL-53(Fe) MOF with a bandgap of 2.72 eV was hybridized with 2.5 wt% rGO, a much enhanced photocatalytic performance was achieved in the degradation of methylene blue (MB), and the degradation

rate constant is 1.57 times that using only MIL-53(Fe) under visible light.

3.3 Chemical sensing

Highly porous materials such as MOFs are inherently good sensing materials because they can pre-concentrate target molecules to a higher level compared to a flat and non-porous substrate.[12] The changes in their properties upon the absorption/attachment of analytes can be measured as a sensing signal. Several signal transduction methods based on their electrical, electrochemical and fluorescence properties can be used for MOF-based sensors.

Although electrical transducing methods have been widely used for sensors, such as chemiresistive sensors and field-effect transistor (FET) sensors, they are less explored for MOFs since the majority of MOFs are insulating. Recently, Nikolina et al. successfully demonstrated a MOF-based chemiresistive sensor by hybridization of insulating Cu-MOF and GO sheets to modulate electrode conductivity. When being exposed to NH$_3$, this hybrid GO/Cu-MOF showed an evident decrease in resistance by doping, indicating its potential use for gas sensing.[86] It is worth noting that for a chemiresistive sensor, the conductivity of a transducing electrode should not be very high. Otherwise, the absorption of a trace amount of analyte is not able to cause a detectable change in electrode conductance. In contrast, for the MOF-based electrochemical sensor, incorporation of insulating MOFs in a highly conductive matrix/network is of great importance in order to achieve good sensing performance. For example, Wang et al. cast the GO/Cu(TPA) composite on a glassy carbon electrode, and then electrochemically reduced the GO to rGO, denoted as electrochemically reduced graphene, EGR. This hybrid electrode was used to detect two drugs, i.e. acetaminophen (ACOP) and dopamine (DA) and achieved detection limits for ACOP and DA as low as 0.36 and 0.21 μM, respectively. This good performance can be attributed to the coupling effect from the high conductivity of EGR and the unique electron mediating action of Cu(TPA).[62]

Since a large number of MOFs are found to be luminescent because the linkers in them contain aromatic subunits that can readily luminesce under light excitation, another important type of MOF-based sensors is based on the fluorescence quenching of luminescent MOF crystals.[87] As is known, the addition of GO or rGO to such system can strongly enhance carrier transportation in the framework, which further amplifies the change of fluorescence signals upon exposure to target molecules. Recently, Jung et al. prepared a GO/MOF nanocomposite through the assembly of azobenzoic acid-functionalized GO and trans-4,4′-stilbene dicarboxylic acid–Zn^{2+} complex, denoted as A–GO/L–Zn^{2+}, which was capable of sensing explosives, such as dinitrotoluene (DNT) and trinitrotoluene (TNT), based on luminescence quenching.[88] Importantly, because the pore size of MOF L–Zn^{2+} is larger than that of DNT molecules but smaller than that of TNT molecules, highly concentrated DNT molecules can pass through the pores of MOF L–Zn^{2+} and interact with it, leading to the selective sensing of DNT (71% quenching) against TNT (20% quenching).

4. Conclusions

Over the past few decades, much progress has been achieved in the synthesis and applications of 2D materials and MOFs. The combination of these two functional materials to form composites has recently shown promise in achieving improved performance in molecular absorption, storage and separation, as well as molecular sensing.

As highlighted in this feature article, an important development in the preparation of 2D material/MOF composites is the usage of surface functionalized graphene sheets as the backbone to construct MOF layers, leading to structural and morphological control of MOF crystals.[55,56] However, in order to understand the mechanism behind the structural directing effect of graphene-based nanosheets, the microstructure of the MOF layer at the graphene/MOF interface should be characterized, which remains a big challenge. One possible approach is to use a focused ion beam to cut the hybrid material and examine the interface under electron microscopy, but special care should be taken to minimize cutting-induced structural changes of the MOF layer.

The exploration of new applications for 2D material/MOF composites should be paid more attention and demand more effort. Currently, most applications of 2D material/MOF composites are within the common application scope for MOFs such as molecule absorption, storage and separation. By taking advantage of the selective permeability of MOFs and the electrical sensing capability of 2D materials, a potential application for 2D material/MOF composites is in sensing of biomaterials, such as DNAs and proteins, based on FET sensors. Another promising application for 2D material/MOF composites is in the development of energy storage devices such as batteries and supercapacitors. However, improvement of the conductivity and stability of most MOF crystals remains a big challenge and requires sustained research effort in molecular design and structural engineering.

Acknowledgements

Notes and references

1 S. L. James, *Chem. Soc. Rev.*, 2003, **32**, 276–288.
2 H. Li, M. Eddaoudi, M. O'Keeffe and O. M. Yaghi, *Nature*, 1999, **402**, 276–279.
3 J. L. C. Rowsell and O. M. Yaghi, *Microporous Mesoporous Mater.*, 2004, **73**, 3–14.
4 M. Eddaoudi, D. B. Moler, H. L. Li, B. L. Chen, T. M. Reineke, M. O'Keeffe and O. M. Yaghi, *Acc. Chem. Res.*, 2001, **34**, 319–330.
5 M. Kurmoo, *Chem. Soc. Rev.*, 2009, **38**, 1353–1379.
6 Y. Cui, Y. Yue, G. Qian and B. Chen, *Chem. Rev.*, 2012, **112**, 1126–1162.
7 J. Lee, O. K. Farha, J. Roberts, K. A. Scheidt, S. T. Nguyen and J. T. Hupp, *Chem. Soc. Rev.*, 2009, **38**, 1450–1459.
8 M. Zhao, Y. Wang, Q. Ma, Y. Huang, X. Zhang, J. Ping, Z. Zhang, Q. Lu, Y. Yu, H. Xu, Y. Zhao and H. Zhang, *Adv. Mater.*, 2015, **27**, 7372–7378.
9 N. L. Rosi, J. Eckert, M. Eddaoudi, D. T. Vodak, J. Kim, M. O'Keeffe and O. M. Yaghi, *Science*, 2003, **300**, 1127–1129.
10 J.-R. Li, R. J. Kuppler and H.-C. Zhou, *Chem. Soc. Rev.*, 2009, **38**, 1477–1504.
11 L. Ma, C. Abney and W. Lin, *Chem. Soc. Rev.*, 2009, **38**, 1248–1256.
12 L. E. Kreno, K. Leong, O. K. Farha, M. Allendorf, R. P. Van Duyne and J. T. Hupp, *Chem. Rev.*, 2012, **112**, 1105–1125.
13 Q. Gong, Z. Hu, B. J. Deibert, T. J. Emge, S. J. Teat, D. Banerjee, B. Mussman, N. D. Rudd and J. Li, *J. Am. Chem. Soc.*, 2014, **136**, 16724–16727.
14 P. Horcajada, T. Chalati, C. Serre, B. Gillet, C. Sebrie, T. Baati, J. F. Eubank, D. Heurtaux, P. Clayette, C. Kreuz, J.-S. Chang, Y. K. Hwang, V. Marsaud, P.-N. Bories, L. Cynober, S. Gil, G. Ferey, P. Couvreur and R. Gref, *Nat. Mater.*, 2010, **9**, 172–178.
15 S. Li and F. Huo, *Nanoscale*, 2015, **7**, 7482–7501.
16 Q.-L. Zhu and Q. Xu, *Chem. Soc. Rev.*, 2014, **43**, 5468–5512.
17 A. Dhakshinamoorthy and H. Garcia, *Chem. Soc. Rev.*, 2012, **41**, 5262–5284.
18 G. Lu, S. Li, Z. Guo, O. K. Farha, B. G. Hauser, X. Qi, Y. Wang, X. Wang, S. Han, X. Liu, J. S. DuChene, H. Zhang, Q. Zhang, X. Chen, J. Ma, S. C. J. Loo, W. D. Wei, Y. Yang, J. T. Hupp and F. Huo, *Nat. Chem.*, 2012, **4**, 310–316.
19 Z. Hu, G. Huang, W. P. Lusting, F. Wang, H. Wang, S. J. Teat, D. Banerjee, D. Zhang and J. Li, *Chem. Commun.*, 2015, **51**, 3045–3048.
20 R. Mas-Balleste, C. Gomez-Navarro, J. Gomez-Herrero and F. Zamora, *Nanoscale*, 2011, **3**, 20–30.
21 M. Xu, T. Liang, M. Shi and H. Chen, *Chem. Rev.*, 2013, **113**, 3766–3798.
22 S. Z. Butler, S. M. Hollen, L. Cao, Y. Cui, J. A. Gupta, H. R. Gutierrez, T. F. Heinz, S. S. Hong, J. Huang, A. F. Ismach, E. Johnston-Halperin, M. Kuno, V. V. Plashnitsa, R. D. Robinson, R. S. Ruoff, S. Salahuddin, J. Shan, L. Shi, M. G. Spencer, M. Terrones, W. Windl and J. E. Goldberger, *ACS Nano*, 2013, **7**, 2898–2926.
23 K. S. Novoselov, A. K. Geim, S. V. Morozov, D. Jiang, Y. Zhang, S. V. Dubonos, I. V. Grigorieva and A. A. Firsov, *Science*, 2004, **306**, 666–669.
24 H. Wang, L. L. Yu, Y. H. Lee, Y. M. Shi, A. Hsu, M. L. Chin, L. J. Li, M. Dubey, J. Kong and T. Palacios, *Nano Lett.*, 2012, **12**, 4674–4680.
25 K. Roy, M. Padmanabhan, S. Goswami, T. P. Sai, G. Ramalingam, S. Raghavan and A. Ghosh, *Nat. Nanotechnol.*, 2013, **8**, 826–830.
26 J. N. Coleman, *et al.*, *Science*, 2011, **331**, 568–571.
27 S. Z. Li, X. Huang and H. Zhang, *Acta Chim. Sin.*, 2015, **73**, 913–923.
28 X. Huang and H. Zhang, *Natl. Sci. Rev.*, 2015, **2**, 19–21.
29 C. L. Tan and H. Zhang, *Nat. Commun.*, 2015, **6**, 7873.
30 H. Zhang, *ACS Nano*, 2015, **9**, 9451–9469.
31 S. Z. Li, X. Huang and H. Zhang, *Acta Chim. Sin.*, 2015, **73**, 913–923.
32 C. H. Hendon, D. Tiana and A. Walsh, *Phys. Chem. Chem. Phys.*, 2012, **14**, 13120–13132.
33 J. Kibsgaard, Z. Chen, B. N. Reinecke and T. F. Jaramillo, *Nat. Mater.*, 2012, **11**, 963–969.
34 M. A. Lukowski, A. S. Daniel, F. Meng, A. Forticaux, L. Li and S. Jin, *J. Am. Chem. Soc.*, 2013, **135**, 10274–10277.
35 I. Ahmed and S. Jhung, *Mater. Today*, 2014, **17**, 136–146.
36 N. Stock and S. Biswas, *Chem. Rev.*, 2012, **112**, 933–969.
37 X. Huang, Z. Zeng and H. Zhang, *Chem. Soc. Rev.*, 2013, **42**, 1934–1946.
38 X. Huang, X. Y. Qi, F. Boey and H. Zhang, *Chem. Soc. Rev.*, 2012, **41**, 666–686.

39 X. Huang, Z. Y. Yin and S. X. Wu, *Small*, 2011, **7**, 1876–1902.
40 C. L. Tan and H. Zhang, *Chem. Soc. Rev.*, 2015, **44**, 2713–2731.
41 H. Li, J. Wu, Z. Y. Yin and H. Zhang, *Acc. Chem. Res.*, 2014, **47**, 1067–1075.
42 X. Huang, C. L. Tan, Z. Y. Yin and H. Zhang, *Adv. Mater.*, 2014, **26**, 2185–2204.
43 Z.-H. Huang, G. Liu and F. Kang, *ACS Appl. Mater. Interfaces*, 2012, **4**, 4942–4947.
44 J.-H. Yang, D. Yang and Y. Li, *Mater. Lett.*, 2014, **130**, 111–114.
45 X. Liu, H. Zhou, Y. Zhang, Y. Liu and A. Yuan, *Chin. J. Chem.*, 2012, **30**, 2563–2566.
46 Z. Bian, X. Zhu, T. Jin, J. Gao, J. Hu and H. Liu, *Microporous Mesoporous Mater.*, 2014, **200**, 159–164.
47 J.-W. Liu, Y. Zhang, X.-W. Chen and J.-H. Wang, *ACS Appl. Mater. Interfaces*, 2014, **6**, 10196–10204.
48 A. Huang, Q. Liu, N. Wang, Y. Zhu and J. Caro, *J. Am. Chem. Soc.*, 2014, **136**, 14686–14689.
49 X. Huang, X. Qi, F. Boey and H. Zhang, *Chem. Soc. Rev.*, 2012, **41**, 666–686.
50 X. Huang, Z. Yin, S. Wu, X. Qi, Q. He, Q. Zhang, Q. Yan, F. Boey and H. Zhang, *Small*, 2011, **7**, 1876–1902.
51 M. Jahan, Q. Bao, J.-X. Yang and K. P. Loh, *J. Am. Chem. Soc.*, 2010, **132**, 14487–14495.
52 C. Scherb, A. Schoedel and T. Bein, *Angew. Chem., Int. Ed.*, 2008, **47**, 5777–5779.
53 S. Li, W. Shi, G. Lu, S. Li, S. C. J. Loo and F. Huo, *Adv. Mater.*, 2012, **24**, 5954–5958.
54 R. Kumar, K. Jayaramulu, T. K. Maji and C. N. R. Rao, *Dalton Trans.*, 2014, **43**, 7383–7386.
55 M. Jahan, Q. Bao and K. P. Loh, *J. Am. Chem. Soc.*, 2012, **134**, 6707–6713.
56 M. Jahan, Z. Liu and K. P. Loh, *Adv. Funct. Mater.*, 2013, **23**, 5363–5372.
57 A. S. Nazarov, V. N. Demin, E. D. Grayfer, A. I. Bulavchenko, A. T. Arymbaeva, H.-J. Shin, J.-Y. Choi and V. E. Fedorov, *Chem. – Asian J.*, 2012, **7**, 554–560.
58 C. Backes, N. C. Berner, X. Chen, P. Lafargue, P. LaPlace, M. Freeley, G. S. Duesberg, J. N. Coleman and A. R. McDonald, *Angew. Chem., Int. Ed.*, 2015, **54**, 2638–2642.
59 Z. Zeng, Z. Yin, X. Huang, H. Li, Q. He, G. Lu, F. Boey and H. Zhang, *Angew. Chem., Int. Ed.*, 2011, **50**, 11093–11097.
60 X. Huang, B. Zheng, Z. Liu, C. Tan, J. Liu, B. Chen, H. Li, J. Chen, X. Zhang, Z. Fan, W. Zhang, Z. Guo, F. Huo, Y. Yang, L.-H. Xie, W. Huang and H. Zhang, *ACS Nano*, 2014, **8**, 8695–8701.
61 P. Wang, H. Li, Q. Gao, P.-Z. Li, X. Yao, L. Bai, N. Kim Truc, R.-Q. Zou and Y. Zhao, *J. Mater. Chem. A*, 2014, **2**, 18731–18735.
62 X. Wang, Q. Wang, Q. Wang, F. Gao, F. Gao, Y. Yang and H. Guo, *ACS Appl. Mater. Interfaces*, 2014, **6**, 11573–11580.
63 Z. Zhao, S. Wang, R. Liang, Z. Li, Z. Shi and G. Chen, *J. Mater. Chem. A*, 2014, **2**, 13509–13512.
64 K. Sumida, D. L. Rogow, J. A. Mason, T. M. McDonald, E. D. Bloch, Z. R. Herm, T.-H. Bae and J. R. Long, *Chem. Rev.*, 2012, **112**, 724–781.
65 L. J. Murray, M. Dinca and J. R. Long, *Chem. Soc. Rev.*, 2009, **38**, 1294–1314.
66 E. Barea, C. Montoro and J. A. R. Navarro, *Chem. Soc. Rev.*, 2014, **43**, 5419–5430.
67 Z.-H. Huang, G. Liu and F. Kang, *ACS Appl. Mater. Interfaces*, 2012, **4**, 4942–4947.
68 S. Gadipelli and Z. X. Guo, *Prog. Mater. Sci.*, 2015, **69**, 1–60.
69 K. Spyrou, D. Gournis and P. Rudolf, *ECS J. Solid State Sci. Technol.*, 2013, **2**, M3160–M3169.
70 R. Kumar, K. Jayaramulu, T. K. Maji and C. N. R. Rao, *Chem. Commun.*, 2013, **49**, 4947–4949.
71 S. Liu, L. Sun, F. Xu, J. Zhang, C. Jiao, F. Li, Z. Li, S. Wang, Z. Wang, X. Jiang, H. Zhou, L. Yang and C. Schick, *Energy Environ. Sci.*, 2013, **6**, 818–823.
72 X. Zhou, W. Huang, J. Miao, Q. Xia, Z. Zhang, H. Wang and Z. Li, *Chem. Eng. J.*, 2015, **266**, 339–344.
73 L. Wang and R. T. Yang, *Energy Environ. Sci.*, 2008, **1**, 268–279.
74 H. Cheng, L. Chen, A. C. Cooper, X. Sha and G. P. Pez, *Energy Environ. Sci.*, 2008, **1**, 338–354.
75 H. Zhou, J. Zhang, J. Zhang, X.-F. Yan, X.-P. Shen and A.-H. Yuan, *Inorg. Chem. Commun.*, 2015, **54**, 54–56.
76 H. Zhou, X. Liu, J. Zhang, X. Yan, Y. Liu and A. Yuan, *Int. J. Hydrogen Energy*, 2014, **39**, 2160–2167.
77 J. Zhang, X. Liu, H. Zhou, X. Yan, Y. Liu and A. Yuan, *RSC Adv.*, 2014, **4**, 28908–28913.
78 L. Li, X. L. Liu, M. Gao, W. Hong, G. Z. Liu, L. Fan, B. Hu, Q. H. Xia, L. Liu, G. W. Song and Z. S. Xu, *J. Mater. Chem. A*, 2014, **2**, 1795–1801.
79 D. M. D'Alessandro, J. R. R. Kanga and J. S. Caddy, *Aust. J. Chem.*, 2011, **64**, 718–722.
80 L. Zhang, Y. Guo, J. Peng, X. Liu, P. Yuan, Q. Yang and C. Li, *Chem. Commun.*, 2011, **47**, 4087–4089.
81 Y. Kobayashi, B. Jacobs, M. D. Allendorf and J. R. Long, *Chem. Mater.*, 2010, **22**, 4120–4122.
82 H. Miyasaka, *Acc. Chem. Res.*, 2013, **46**, 248–257.
83 H. A. Becerril, J. Mao, Z. Liu, R. M. Stoltenberg, Z. Bao and Y. Chen, *ACS Nano*, 2008, **2**, 463–470.
84 L. Xu, G. Zhang, J. Chen, Y. Zhou, G. e. Yuan and F. Yang, *J. Power Sources*, 2013, **240**, 101–108.
85 Y. Zhang, G. Li, H. Lu, Q. Lv and Z. Sun, *RSC Adv.*, 2014, **4**, 7594–7600.
86 K. S. Nikolina, A. Travlou, E. Rodríguez-Castellón and T. J. Bandosz, *J. Mater. Chem. A*, 2015, **3**, 13.
87 Z. Hu, B. J. Deibert and J. Li, *Chem. Soc. Rev.*, 2014, **43**, 5815–5840.
88 J. H. Lee, J. Jaworski and J. H. Jung, *Nanoscale*, 2013, **5**, 8533–8540.